JBIC Journal of Biological Inorganic Chemistry
https://doi.org/10.1007/s00775-018-1567-3

ORIGINAL PAPER

Impact of various lipophilic substituents on ruthenium(II), rhodium(III) and iridium(III) salicylaldimine-based complexes: synthesis, in vitro cytotoxicity studies and DNA interactions

Irwin Cassells[1] · Tameryn Stringer[1] · Alan T. Hutton[1] · Sharon Prince[2] · Gregory S. Smith[1]

Received: 14 March 2018 / Accepted: 28 April 2018

Abstract
A series of bidentate salicylaldimine ligands was prepared and reacted with either $[RuCl(\mu\text{-}Cl)(p\text{-cymene})]_2$, $[RhCl(\mu\text{-}Cl)(Cp^*)]_2$ or $[IrCl(\mu\text{-}Cl)(Cp^*)]_2$. All of the compounds were characterised using an array of spectroscopic and analytical techniques, namely, nuclear magnetic resonance (NMR) spectroscopy, infrared (IR) spectroscopy and mass spectrometry. Single crystal X-ray diffraction (XRD) was used to confirm the bidentate coordination mode of the salicylaldimine ligand to the metal centre. The platinum group metal (PGM) complexes were screened against the MCF7 breast cancer cell line. The ruthenium and iridium salicylaldimine complexes showed comparable or greater cytotoxicity than cisplatin against the MCF7 cancer cells, as well as greater cytotoxicity than their rhodium counterparts. Three of the salicylaldimine complexes showed potent activity in the range 18–21 μM. Two of these complexes had a greater affinity for cancerous cells than for CHO non-cancerous cells (SI > 4). Preliminarymechanistic studies suggest that the ruthenium complexes undergo solvation prior to 5′-GMP binding, whereas the iridium complexes were inert to the solvation process.

Crystallographic data: CCDC 1572708 (11), CCDC 1572709 (12), CCDC 1572710 (13).

✉ Gregory S. Smith
Gregory.Smith@uct.ac.za

[1] Department of Chemistry, University of Cape Town, Rondebosch 7701, South Africa

[2] Department of Human Biology, University of Cape Town, Medical School, Observatory 7925, South Africa

Published online: 30 May 2018

Graphical abstract

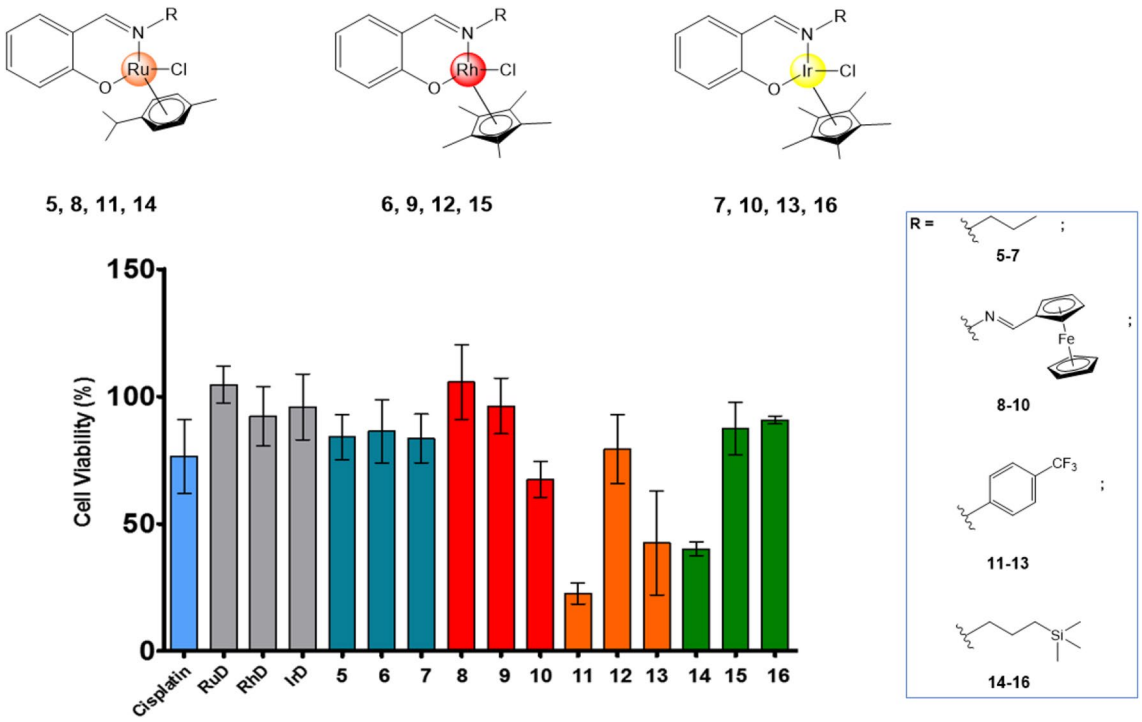

Keywords Salicylaldimine · Ruthenium–arene · Rhodium · Iridium · Anticancer activity

Introduction

Since the discovery of the anticancer properties of cisplatin by Rosenberg [1, 2], metal-based treatments have been of interest to researchers. Cisplatin is a frequently used metal-based drug against ovarian and testicular cancers [3]. Considering the high levels of toxicity and unfavourable side effects of cisplatin, a range of biologically active organometallic complexes, such as the half-sandwich piano stool Ru(II) complexes [4, 5], has been investigated to treat various cancers with reduced side effects. These platinum group metal (PGM) complexes have shown exceptional promise, with the development of a few complexes, such as $[(\eta^6\text{-}p\text{-cymene})Ru(en)Cl]PF_6$ and $[(\eta^6\text{-}p\text{-cymene})Ru(PTA)Cl_2]$ (where en = ethylenediamine and PTA = 1,3,5-triaza-7-phosphaadamantane), continuing to the pre-clinical stage [6, 7]. Of these, piano stool structures with either an η^6-*p*-cymene or η^5-pentamethylcyclopentadienyl (Cp*) ligand, in general, have shown the most promise. The dimeric precursors ($[MCl_2(p\text{-cymene or Cp*})]_2$, M = platinum group metal) of these complexes have been shown to be biologically inactive, strongly suggesting that the activity of these complexes is ligand dependent [8, 9]. Recently, McGowan and co-workers have observed an increase in activity of these organometallic complexes through the splitting of the metal dimers using *N*,*N*-, *N*,*O*- or *O*,*O*-bidentate ligands, where complexes containing *N*,*O*-chelates were found to exhibit the greatest activity [8, 9].

Salicylaldimine ligands (*N*,*O*-chelates) are versatile and easily functionalised building blocks for small molecules and larger macromolecular metal complexes and selected examples currently used in a wide range of biological

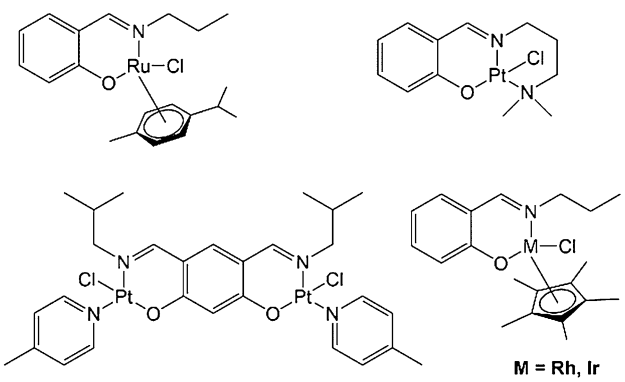

Fig. 1 Selected salicylaldimine structures that have shown promise in biological applications [13–15, 19, 20]

applications are shown in Fig. 1 [10–18]. Salicylaldimine compounds enhance the distribution of the metal into cell organelles and interrupt DNA processes, increasing the activity of the complex [16, 17]. Various salicylaldimine PGM complexes have been reported to show moderate or low activity against human ovarian cancer cell lines, A2780 and A2780cis [13, 19]. However, in other cell lines, namely MCF7 (human breast carcinoma) and A549 (lung cancer), similar complexes show comparable activity to cisplatin [15, 20]. Three lipophilic groups of interest for this study have been the ferrocenyl, trifluoromethyl and trimethylsilane groups, which have been reported to show biological activity [18, 21–23]. Ferrocenyl groups have the ability to promote single electron redox transfers and have shown high cytotoxicity in various invasive cancer cell lines in vitro [24, 25]. Fluorine groups are resistant to chemical degradation [21], favourable for enzyme inhibition [21, 26], and have shown inhibition of tumour growth at third- and fourth-line cancers [27]. In a recent study, an increased activity in chloroquine-sensitive (NF54) and chloroquine-resistant (Dd2) *Plasmodium falciparum* strains of the malaria parasite was discovered for organosilane complexes in comparison to carbon analogues, further supporting its relevance in drug discovery [22, 23].

The combination of salicylaldimine ligands with PGM dimeric precursors is thus a prolific area of research and a popular strategy in drug design, and we and other researchers have previously reported on this strategy [13, 18, 19, 22, 23]. This study details the synthesis and characterisation of trifluoromethane- and organosilane-derivatised salicylaldimine complexes, as well as ferrocenyl- and propylsalicylaldimine complexes, with a particular focus on the influence of these lipophilic substituents on the biological activity of salicylaldimine-containing metal complexes.

Experimental

Materials and methods

Reagents were purchased from either Sigma-Aldrich or Merck and used as received. Solvents (from KIMIX) were dried using molecular sieves. Nuclear magnetic resonance (NMR) spectra were recorded on a Bruker Topspin GmbH (^{1}H: 400.22 MHz, ^{13}C{^{1}H}: 100.65 MHz, ^{19}F{^{1}H}: 376.58 MHz, ^{31}P{^{1}H}: 162.01 MHz) or a Varian Mercury XR300 (^{1}H: 300.08 MHz) spectrometer, with a Bruker Biospin GmbH casing and sample injector at 30 °C. Chemical shifts were reported using tetramethylsilane (TMS) as the internal standard. Infrared (IR) absorptions were measured on a Perkin-Elmer Spectrum One FT-IR spectrometer using attenuated total reflection (ATR) in the solid state. Elemental analysis was carried out using a Fisons EA 110 CHNS elemental analyser. Electron impact (EI) mass spectrometry was carried out on a JEOL GCmate II mass spectrometer (**1**–**10**). Electrospray ionisation (ESI) mass spectrometry was carried out on a Waters API Quattro instrument in the positive-ion mode for complexes **11**–**16**. Melting points were determined using a Büchi melting point B-540 apparatus and are uncorrected. Dimeric precursors [28, 29], compounds **1–3** [19, 30] and **5**–**10** [18, 19] were synthesised using published methods.

Synthesis of (trimethylsilyl)propylsalicylaldimine ligand (4)

Salicylaldehyde (0.437 g, 3.58 mmol) and 3-aminopropyltrimethylsilane (0.548 g, 4.17 mmol) were stirred in diethyl ether under an inert atmosphere for 16 h. The resulting yellow solution was then washed with water (3 × 15 mL) to remove the excess amine. The organic fractions were collected, dried over anhydrous magnesium sulfate, filtered and the solvent removed to yield a yellow oil (**4**). Yield: 0.783 g (93%). ^{1}H NMR (400 MHz, $CDCl_3$): δ_H (ppm) = 0.02 (9H, s, CH_3), 0.53–0.59 (2H, m, CH_2), 1.66–1.76 (2H, m, CH_2), 3.60 (2H, t, ^{3}J = 7.4 Hz, CH_2), 6.89 (1H, t, ^{3}J = 7.4 Hz, Ar–H), 6.99 (1H, d, ^{3}J = 8.3 Hz, Ar–H), 7.26–7.35 (2H, m, Ar–H), 8.35 (1H, s, HC=N), 13.70 (1H, s, OH). ^{13}C{^{1}H} NMR (100 MHz, $CDCl_3$): δ_C (ppm) = − 1.79 (CH_3), 14.14 (CH_2), 25.51 (CH_2), 62.68 (CH_2), 117.03 (Ar), 118.30 (Ar), 118.81 (Ar), 131.04 (Ar), 131.97 (Ar), 161.47 (Ar), 164.42 (C_{imine}). EI-MS *m*/*z* 235.1259 (100%, $[M]^+$). Analysis Calc. for $C_{13}H_{21}NOSi$: C, 66.33; H, 8.99; N, 5.95. Found: C, 66.31; H, 9.20; N, 5.96.

General procedure for the synthesis of complexes 11–13

Ligand **3** and triethylamine were stirred together in dichloromethane for 60 min. To the yellow solution, [RuCl(μ-Cl)(*p*-cymene)]$_2$, [RhCl(μ-Cl)(Cp*)]$_2$ or [IrCl(μ-Cl)(Cp*)]$_2$ was added and stirred for an additional 18 h. The resulting solution was washed with water (3 × 15 mL) in a separating funnel, and the organic fractions collected and dried using anhydrous magnesium sulfate. After removal of the drying agent by filtration, the solvent was removed and the residue taken up in a minimal amount of dichloromethane, to which diethyl ether was added to precipitate the desired complex.

Data for ruthenium–CF_3 complex (11)

Compound **3** (0.0875 g, 0.330 mmol) and triethylamine (0.1 mL, 0.717 mmol) were reacted with [RuCl(μ-Cl)(*p*-cymene)]$_2$ (0.101 g, 0.164 mmol). Complex **11** was isolated as a brown powder. Yield: 0.0833 g (47%). Melting point: 226 °C dec. with melting. ^{1}H NMR (400 MHz,

$CDCl_3$): δ_H (ppm) = 1.14 (3H, d, ^3J = 6.8 Hz, CH_3), 1.19 (3H, d, ^3J = 6.8 Hz, CH_3), 2.13 (3H, s, CH_3), 2.64 (1H, sept, ^3J = 6.8 Hz, CH), 4.25 (1H, d, ^3J = 5.4 Hz, Ar_{pcy}), 5.01 (1H, d, ^3J = 5.4 Hz, Ar_{pcy}), 5.28 (1H, d, ^3J = 6.4 Hz, Ar_{pcy}), 5.36 (1H, d, ^3J = 6.4 Hz, Ar_{pcy}), 6.42–6.44 (1H, m, Ar–H), 6.95 (1H, dd, ^3J = 7.8 Hz, ^4J = 1.8 Hz, Ar–H), 6.99–7.01 (1H, m, Ar–H), 7.22–7.27 (1H, m, Ar–H), 7.72–7.74 (3H, m, Ar–H + HC=N), 7.80–7.82 (2H, m, Ar–H). $^{13}C\{^1H\}$ NMR (100 MHz, $CDCl_3$): δ_C (ppm) = 18.47 (CH_3), 21.68 (CH_3), 22.66 (CH_3), 30.41 (CH), 80.25 (C_{pcy}), 83.08 (C_{cym}), 83.25 (C_{pcy}), 86.59 (C_{pcy}), 98.31 (C_{pcy}), 101.74 (C_{pcy}), 114.50 (Ar), 117.95 (Ar), 122.91 (Ar), 123.85 (q, $^1J_{C–F}$ = 270.1 Hz, CF_3), 124.38 (Ar), 126.14 (q, $^3J_{C–F}$ = 2.9 Hz, Ar), 129.12 (q, $^2J_{C–F}$ = 30.0 Hz, Ar), 135.46 (Ar), 136.08 (Ar), 160.83 (Ar), 164.6 (C_{imine}), 165.66 (Ar). $^{19}F\{^1H\}$ NMR (376 MHz, $CDCl_3$): δ_F (ppm) = − 62.21 (s). IR (ATR): ν/cm^{-1} = 1615 (C=N). ESI–MS (HR) *m/z* 238.1773 (100%, $[M+H+Na]^{2+}$ requires 238.2999). Analysis Calc. for $C_{24}H_{23}ClF_3NORu$: C, 53.88; H, 4.33; N, 2.62. Found: C, 53.55; H, 4.14; N, 2.24.

Data for rhodium–CF_3 complex (12)

Compound **3** (0.0866 g, 0.327 mmol) and triethylamine (0.1 mL, 0.717 mmol) were reacted with [RhCl(μ-Cl)(Cp*)]$_2$ (0.101 g, 0.167 mmol). Complex **12** was isolated as an orange powder. Yield: 0.132 g (75%). Melting point: 241 °C dec. with melting. ^1H NMR (400 MHz, $CDCl_3$): δ_H (ppm) = 1.35 (15H, s, CH_3), 6.43–6.47 (1H, m, Ar–H), 7.01–7.07 (2H, m, Ar–H), 7.24–7.28 (1H, m, Ar–H), 7.69 (2H, d, ^3J = 8.3 Hz, Ar–H), 7.94 (1H, s, HC=N), 8.01 (2H, d, ^3J = 8.1 Hz, Ar–H). $^{13}C\{^1H\}$ NMR (100 MHz, $CDCl_3$): δ_C (ppm) = 8.42 (CH_3), 93.67 (d, $J_{C–Rh}$ = 8.8 Hz, Cp*), 114.33 (Ar), 119.21 (Ar), 123.96 (q, $^1J_{C–F}$ = 272.2 Hz, CF_3), 124.35 (Ar), 125.22 (Ar), 125.83 (q, $^3J_{C–F}$ = 3.7 Hz, Ar), 128.90 (q, $^2J_{C–F}$ = 32.5 Hz, Ar), 135.51 (Ar), 135.81 (Ar), 157.15 (Ar), 165.10 (C_{imine}), 166.80 (Ar). $^{19}F\{^1H\}$ NMR (376 MHz, $CDCl_3$): δ_F (ppm) = − 62.15 (s). IR (ATR): ν/cm^{-1} = 1603 (C=N). ESI–MS (HR) *m/z* 502.0861 (100%, $[M-Cl]^+$ requires 502.0865). Analysis Calc. for $C_{24}H_{24}ClF_3NORh$: C, 53.60; H, 4.50; N, 2.60. Found: C, 53.33; H, 4.31; N, 2.48.

Data for iridium–CF_3 complex (13)

Compound **3** (0.0685 g, 0.258 mmol) and triethylamine (0.1 mL, 0.717 mmol) were reacted with [IrCl(μ-Cl)(Cp*)]$_2$ (0.0998 g, 0.125 mmol). Complex **13** was isolated as an orange powder. Yield: 0.108 g (69%). Melting point: 243 °C dec. with melting. ^1H NMR (400 MHz, $CDCl_3$): δ_H (ppm) = 1.33 (15H, s, CH_3), 6.46 (1H, t, ^3J = 7.2 Hz, Ar–H), 6.97 (1H, d, ^3J = 8.6 Hz, Ar–H), 7.11 (1H, d, ^3J = 7.6 Hz, Ar–H), 7.37 (1H, t, ^3J = 7.2 Hz, Ar–H), 7.67 (2H, d, ^3J = 8.1 Hz, Ar–H), 7.85 (2H, d, ^3J = 8.1 Hz, Ar–H), 8.01 (1H, s, HC=N). $^{13}C\{^1H\}$ NMR (100 MHz, $CDCl_3$): δ_C (ppm) = 8.43 (CH_3), 85.81 (Cp*), 115.21 (Ar), 120.09 (Ar), 123.53 (Ar), 123.80 (q, $^1J_{C–F}$ = 272.6 Hz, CF_3), 125.45 (Ar), 125.57 (q, $^2J_{C–F}$ = 3.7 Hz, Ar), 129.77 (q, $^2J_{C–F}$ = 32.5 Hz, Ar), 134.65 (Ar), 135.77 (Ar), 159.12 (Ar), 161.41 (C_{imine}), 164.34 (Ar). $^{19}F\{^1H\}$ NMR (376 MHz, $CDCl_3$): δ_F (ppm) = − 62.17 (s). IR (ATR): ν/cm^{-1} = 1615 (C=N). ESI–MS (HR) *m/z* 592.1528 (80%, $[M-Cl]^+$ requires 592.1439). Analysis Calc. for $C_{24}H_{24}ClF_3NOIr$: C, 45.97; H, 3.86; N, 2.23. Found: C, 45.33; H, 3.87; N, 1.95.

General procedure for the synthesis of complexes 14–16

[RuCl(μ-Cl)(*p*-cymene)]$_2$, [RhCl(μ-Cl)(Cp*)]$_2$ or [IrCl(μ-Cl)(Cp*)]$_2$ was added to a stirring solution of triethylamine and **4** in diethyl ether and stirred for 18 h at room temperature. The excess dimer and triethylammonium chloride that formed were filtered and a red or orange solution was obtained. The solvent was removed in vacuo and the residue washed with *n*-pentane to yield the desired complexes.

Data for ruthenium–silane complex (14)

Compound **4** (0.0876 g, 0.372 mmol) and triethylamine (0.1 mL, 0.717 mmol) were reacted with [RuCl(μ-Cl)(*p*-cymene)]$_2$ (0.137 g, 0.224 mmol). Complex **14** was isolated as a dark brown crystalline powder. Yield: 0.0884 g (46%). Melting point: 146 °C dec. with melting. ^1H NMR (400 MHz, $CDCl_3$): δ_H (ppm) = 0.05 (9H, s, CH_3), 0.44–0.54 (1H, m, CH_2), 0.60–0.70 (1H, m, CH_2), 1.15 (3H, d, ^3J = 6.9 Hz, CH_3), 1.25 (3H, d, ^3J = 7.1 Hz, CH_3), 1.84–1.96 (1H, m, CH_2), 2.00–2.14 (1H, m, CH_2), 2.22 (3H, s, CH_3), 2.79 (1H, sept, ^3J = 7.0 Hz, CH), 3.94–4.04 (1H, m, CH_2), 4.20–4.29 (1H, m, CH_2), 5.02 (1H, d, ^3J = 8.6 Hz, Ar_{pcy}), 5.39 (3H, m, Ar_{pcy}), 6.38–6.42 (1H, m, Ar–H), 6.90–6.97 (2H, m, Ar–H), 7.13–7.19 (1H, m, Ar–H), 7.67 (1H, s, HC=N). $^{13}C\{^1H\}$ NMR (100 MHz, $CDCl_3$): δ_C (ppm) = − 1.70 (CH_3), 14.13 (CH_2), 18.49 (CH_3), 21.61 (CH_3), 22.70 (CH_3), 25.74 (CH_2), 30.46 (CH), 72.69 (CH_2), 80.11 (Ar_{pcy}), 82.07 (Ar_{pcy}), 83.25 (Ar_{pcy}), 85.86 (Ar_{pcy}), 97.24 (Ar_{pcy}), 101.57 (Ar_{pcy}), 113.97 (Ar), 119.21 (Ar), 122.22 (Ar), 134.33 (Ar), 134.46 (Ar), 163.34 (C_{imine}), 164.92 (Ar). IR (ATR): ν/cm^{-1} = 1618 (C=N). ESI–MS (HR) *m/z* 470.1460 (100%, $[M-Cl]^+$ requires 470.1459). Analysis Calc. for $C_{23}H_{34}ClNORuSi{\cdot}0.6H_2O$: C, 53.42; H, 6.89; N, 2.71. Found: C, 53.17; H, 6.81; N, 2.47.

Data for rhodium–silane complex (15)

Compound **4** (0.0997 g, 0.423 mmol) and triethylamine (0.1 mL, 0.717 mmol) were reacted with [RhCl(μ-Cl)(Cp*)]$_2$ (0.126 g, 0.204 mmol). Complex **15** was isolated as a red powder. Yield: 0.101 g (49%). Melting point:

166 °C dec. with melting. ^{1}H NMR (400 MHz, $CDCl_3$): δ_H (ppm) = − 0.01 (9H, s, CH_3), 0.48–0.52 (2H, m, CH_2), 1.53 (15H, s, CH_3), 1.68–1.71 (1H, m, CH_2), 2.15–2.25 (1H, m, CH_2), 3.80–4.03 (2H, m, CH_3), 6.41–6.45 (1H, m, Ar–H), 6.92 (1H, d, ^{3}J = 8.4 Hz, Ar–H), 7.01 (1H, dd, ^{3}J = 7.7 Hz, ^{4}J = 1.7 Hz, Ar–H), 7.13–1.17 (1H, m, Ar–H), 7.78 (1H, s, HC=N). ^{13}C{^{1}H} NMR (100 MHz, $CDCl_3$): δ_C (ppm) = − 1.72 (CH_3), 8.61 (CH_3), 14.02 (CH_2), 25.28 (CH_2), 66.97 (CH_2), 92.65 (d, $^{1}J_{C-Rh}$ = 8.1 Hz, Cp*), 114.05 (Ar), 121.92 (Ar), 123.70 (Ar), 133.71 (Ar), 133.90 (Ar), 162.31 (C_{imine}), 166.60 (Ar). IR (ATR): ν/cm^{-1} = 1621 (C=N). ESI–MS (HR) m/z 472.1551 (100%, [M−Cl]$^{+}$ requires 472.1543). Analysis Calc. for $C_{23}H_{35}ClNORhSi{\cdot}0.2Et_2O$: C, 54.68; H, 7.13; N, 2.68. Found: C, 55.32; H, 6.86; N, 2.39.

Data for iridium–silane complex (16)

Compound **4** (0.0337 g, 0.143 mmol) and triethylamine (0.1 mL, 0.717 mmol) were reacted with [IrCl(μ-Cl)(Cp*)]$_2$ (0.0697 g, 0.0875 mmol). Complex **16** was isolated as a fine yellow powder. Yield: 0.0478 g (56%). Melting point: 158 °C dec. with melting. ^{1}H NMR (400 MHz, $CDCl_3$): δ_H (ppm) = 0.03 (9H, s, CH_3), 0.51 (2H, br m, CH_2), 1.56 (15H, s, CH_3), 1.70–1.93 (1H, br m, CH_2), 1.94–2.17 (1H, br m, CH_2), 3.75–4.20 (2H, br m, CH_2), 6.40–6.44 (1H, m, Ar–H), 6.87–6.90 (1H, m, Ar–H), 7.04 (1H, dd, ^{3}J = 7.7 Hz, ^{4}J = 1.8 Hz, Ar–H), 7.21–7.25 (1H, m, Ar–H), 7.75 (1H, s, HC=N). ^{13}C{^{1}H} NMR (100 MHz, $CDCl_3$): δ_C (ppm) = − 1.70 (CH_3), 8.83 (CH_3), 14.03 (CH_2), 25.45 (CH_2), 69.86 (CH_2), 84.64 (Cp*), 114.79 (Ar), 121.88 (Ar), 122.71 (Ar), 133.15 (Ar), 134.00 (Ar), 159.72 (C_{imine}), 165.19 (Ar). IR (ATR): ν/cm^{-1} = 1619 (C=N). ESI–MS (HR) m/z 562.2133 (100%, [M−Cl]$^{+}$) requires 562.2117. Analysis Calc. for $C_{23}H_{35}ClIrNOSi{\cdot}0.2Et_2O$: C, 46.70; H, 6.09; N, 2.29. Found: C, 47.11; H, 5.86; N, 1.89.

X-ray crystallography

Single crystal X-ray diffraction data were collected on a Bruker KAPPA APEX II DUO diffractometer using graphite-monochromated Mo-Kα radiation (λ = 0.71073Å). The temperature was controlled using an Oxford Cryostream cooling system (Oxford Cryostat). Data scaling and absorption correction were performed using SAINT [31] and SADABS [32]. Structures were solved by direct methods using SHELXS-97 and refined by full-matrix least-squares methods based on F^2 using SHELXL-2014 [33, 34] with X-Seed used as the graphical interface. X-Seed and POV-Ray were used to prepare molecular graphic images. The crystallographic data for complexes **11**–**13** are presented in Table 2.

Cytotoxicity studies

Cells (MCF7) were seeded in a 96-well plate (5000 cells per well) and after 48 h treated with either vehicle (1.0 μM in DMSO) or complexes **5**–**16** and cisplatin at 20 μM for 48 h. The impact of these complexes on cell viability of these complexes was assessed using 3-(4,5-dimethylthiazol-2-yl)-2,5-diphenyltetrazolium bromide (MTT) assay, as described in the literature [35]. The absorbance at 550 nm was determined for each well using a spectrophotometer (RTQ2100C Microplate Reader, Ryto, China) and normalised to the RPMI medium absorbance. This experiment was performed three times in quadruplicate, and then the mean cell viability determined using GraphPad Prism version 5.0. For IC_{50} (concentration required for 50% viability) determination of **11**, **13** and **14**, cells were treated using concentrations of 5–25 μM on three occasions in quadruplicate. For the Chinese hamster ovarian (CHO) cells, 3000 cells per well were plated and tested at concentrations of 0.001, 0.01, 0.1, 1, 10 and 100 μg/mL.

NMR stability studies in DMSO and interactions with DNA model 5′-GMP

The stability of complexes **11** and **13** was investigated by ^{1}H NMR experiments in which approximately 3.0 mg of the complex was dissolved in 0.5 mL DMSO-d_6, 0.5 mL of 50% H_2O in DMSO-d_6 (by volume) or 150 mM NaCl solution in 0.5 mL of 50% H_2O in DMSO-d_6 (by volume). The NMR samples were heated and maintained at 37 °C between sampling. ^{1}H NMR spectra were collected at 0, 24 and 48 h after the initial sample preparation. Similarly, approximately 3.0 mg of sodium 5′-guanosine monophosphate was dissolved in 0.25 mL H_2O, and mixed with 3.0 mg of complex in 0.25 mL DMSO-d_6. The sample was monitored at 0, 24 and 48 h after preparation while heating to 37 °C between NMR sampling.

Results and discussion

Synthesis and characterisation

A small series of four salicylaldimine ligands (Scheme 1) was synthesised following published literature methods [19, 30]. Salicylaldehyde was reacted with either *n*-propylamine, 4-trifluoroaniline or 3-aminopropyltrimethylsilane via a Schiff-base condensation reaction to afford ligands **1**, **3** and **4**. The Schiff-base products were isolated as either viscous yellow oils (**1** and **4**) or an amorphous yellow powder (**3**) in

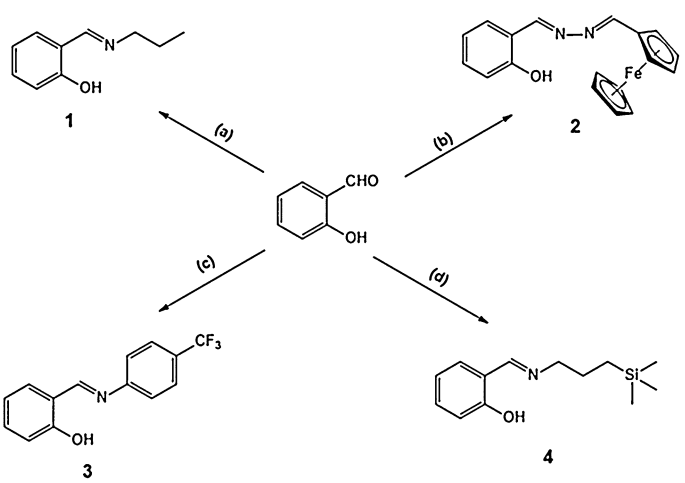

Scheme 1 Synthesis of ligands **1**–**4**. **a** *n*-Propylamine/dichloromethane/18 h/r.t. **b** (i) $NH_2NH_2{\cdot}xH_2O$/1 h/r.t, (ii) ferrocenecarboxaldehyde/ethanol/18 h/r.t. **c** 4-(Trifluoromethyl)aniline/2 h/r.t. **d** 3-Aminopropyltrimethylsilane/16 h/Ar(g)/r.t

high yields (91–93%). Compound **2** was synthesised using salicylaldehyde hydrazone and ferrocenecarboxaldehyde, and was isolated as a deep red amorphous solid in high yield (75%) [18].

Analysis of the ^{1}H NMR spectra of compounds **1**–**4** revealed the absence of the aldehyde resonance at δ_H 9.87 ppm (salicylaldehyde), confirming the successful synthesis of the Schiff-base ligands. The presence of a singlet in the ^{1}H NMR spectra of **1**–**4**, in the region of δ_H 8.3–8.7 ppm, confirmed the presence of the imine functionality. In the ^{13}C{^{1}H} NMR spectra of **1**–**4**, signals for the C-OH carbon were observed at δ_C 161 ppm. In **3**, C-F coupling was observed for the carbons closest to the fluorine atoms. Coupling constants for $^1J_{C–F}$, $^2J_{C–F}$ and $^3J_{C–F}$ were observed and found to be 272.0, 32.5 and 3.7 Hz, respectively, and these signals were observed as quartets. A single peak was observed in the ^{19}F{^{1}H} NMR spectrum of **3** at δ_F −62 ppm. The IR spectra of compounds **1**–**4** displayed absorption bands for the imine C=N between 1585 and 1618 cm^{-1}, providing further support that the proposed compounds had been synthesised.

A series of *N*,*O*-salicylaldimine Ru(II), Rh(III) and Ir(III) complexes, **5**–**16**, was synthesised using the aforementioned ligands via a bridge splitting reaction of [RuCl(μ-Cl)

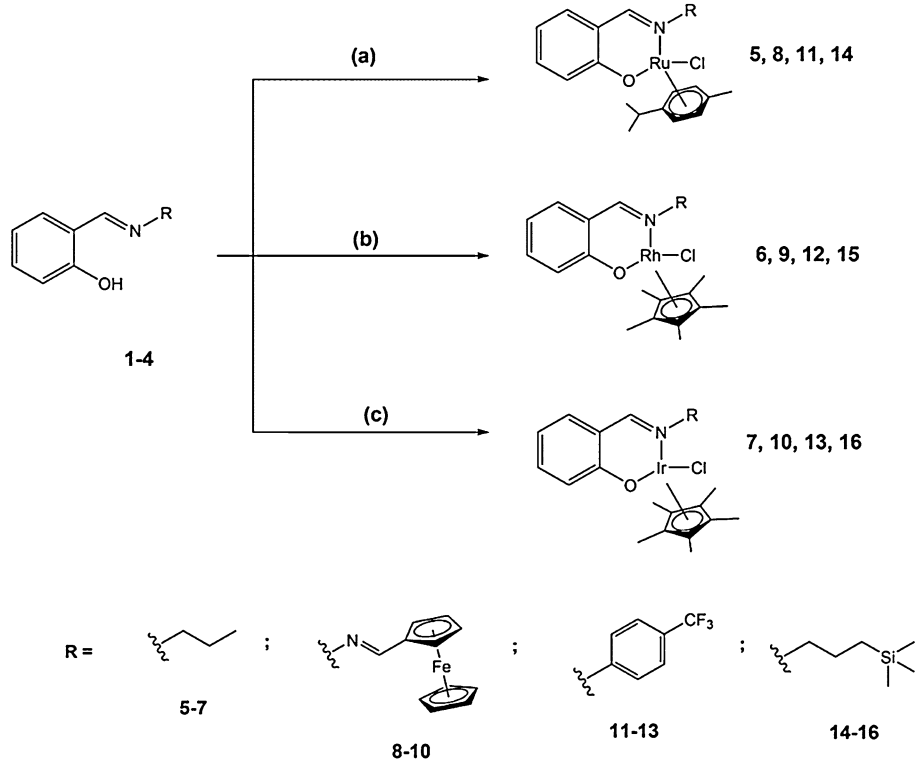

Scheme 2 Synthesis of complexes **5**–**16**. **a** **1**–**4**/[RuCl(μ-Cl)(*p*-cymene)]$_2$/Et$_3$N/r.t. **b** **1**–**4**/[RhCl(μ-Cl)(Cp*)]$_2$/Et$_3$N/r.t. **c** **1**–**4**/[IrCl(μ-Cl)(Cp*)]$_2$/Et$_3$N/r.t

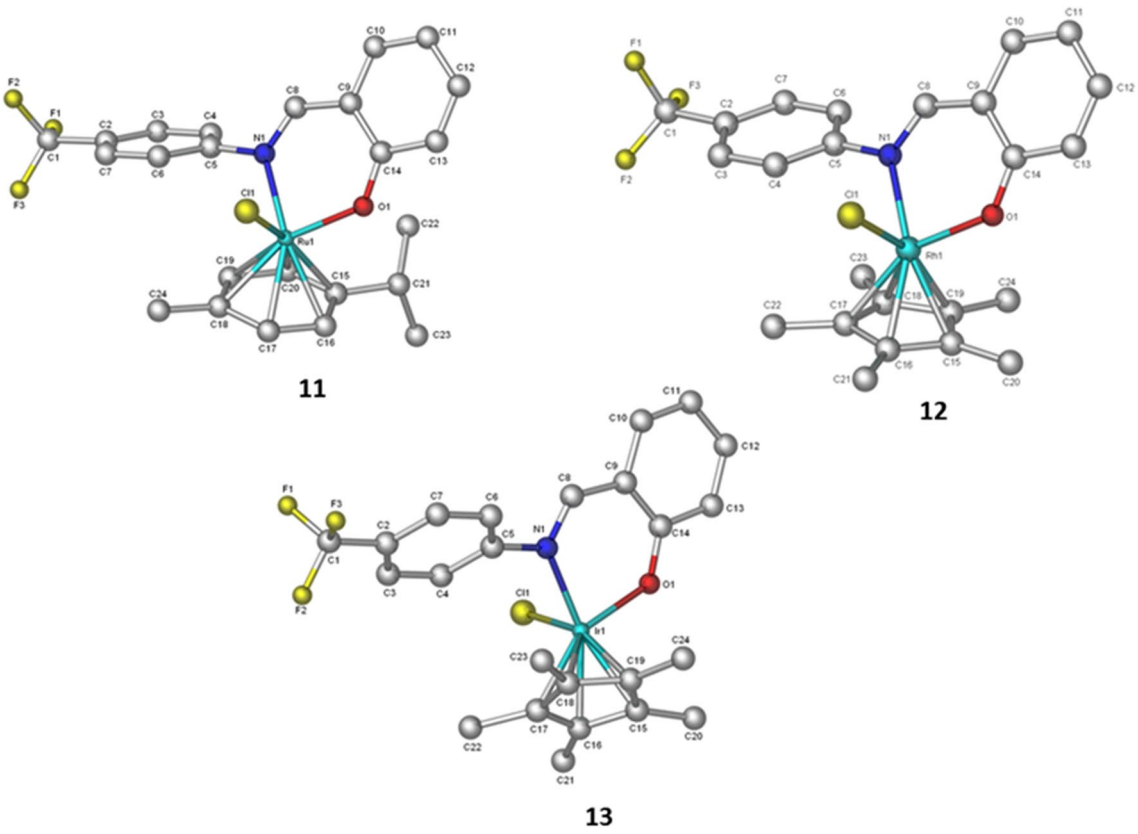

Fig. 2 Molecular structures of **11**, **12** and **13**. Hydrogen atoms are omitted for clarity

(*p*-cymene)]$_2$, [RhCl(μ-Cl)(Cp*)]$_2$ or [IrCl(μ-Cl)(Cp*)]$_2$ (Scheme 2). Complexes **5**–**7**, **8**–**10**, **11**–**13** and **14**–**16** were synthesised by reacting **1**–**4** in the presence of triethylamine to deprotonate the hydroxyl group and subsequent reaction with the corresponding metal dimer to form the desired (*N*,*O*)-complexes. Complexes **5**–**10** were synthesised according to literature methods [18, 19]. Complexes **11**–**13** were synthesised using the method reported by Smith et al. [19] and **14**–**16** were synthesised in diethyl ether. Complexes were isolated as amorphous powders in moderate yields.

All spectroscopic and analytical data for **5**–**10** were in accordance with the reported literature [18, 19]. In the ^{1}H NMR spectra of **11**–**13**, an upfield shift in the imine proton signal was observed (δ_H 7.7–8.0 ppm) when compared to the free ligand (δ_H 8.68 ppm). Minute shifts in the (trifluoromethyl)phenyl group suggest little to no interaction with the *p*-cymene or Cp* ligands. In the ^{13}C{^{1}H} NMR spectra of **11**–**13**, a distinct downfield shift of the carbon signals adjacent to the oxygen from δ_C 151 to 160–161 ppm confirmed bonding of the oxygen atom to the metal centre. The imine carbon resonance exhibited minor shifts from δ_C 164 to 161–164 ppm. This was further confirmed using ^{19}F{^{1}H} NMR spectroscopy. As observed in **3**, a single resonance was observed at δ_F − 62 ppm in the spectra of **11**–**13**, which supports the notion of a single fluorine species. The ^{1}H NMR spectra of **14**–**16** indicate the chirality of the complexes, and a similar phenomenon is observed in the spectra of complexes **5**–**7**. Each CH_2 proton of the propyl chain was observed at two separate chemical shifts and integrated for a solitary proton. An upfield shift of the imine signal from δ_H 8.35 to 7.6–7.6 ppm is indicative of a change in the chemical environment of the imine substructure. No hydroxyl signal was observed in the ^{1}H NMR spectra, strongly suggesting that the ligand was deprotonated in the synthesis process. As found for complexes **5**–**7**, resonances for the imine and CO-M carbon atoms in the ^{13}C{^{1}H} NMR spectra were observed to have an upfield or downfield shift, respectively. In the IR spectra, an overall trend indicating a shift to lower wavenumbers of the C=N stretching vibration from the spectra of the metal-free ligands (~ 1630 cm^{-1}) to the PGM complexes (~ 1615 cm^{-1}) was observed, supporting the notion of coordination to the *N*,*O*-chelate.

X-ray crystallography

Single crystal XRD is a useful technique to understand the molecular structures of complexes. Single crystals of **11**–**13** were obtained by slow diffusion of diethyl ether into methanol and the structures of these complexes were elucidated. These complexes crystallised in the $P2_1/c$ space group with four molecules present in each unit cell. The geometry of the metal is consistent with the proposed piano stool geometry, with the angles between the N, O and Cl donor atoms ranging between 85° and 89°, indicative of a pseudo-tetrahedral arrangement (Fig. 2). This is consistent with the data obtained for complex **5**, reported by Smith et al. [19]. The two phenyl groups are observed to be ~ 90° in relation to each other. A six-membered ring is formed between the (*N*,*O*)-chelating ligand and the metal centre, further supporting the proposed bidentate structure. Bond distances between the metal and chlorido ligand are 20% larger in comparison to the *N*,*O*-chelate and the arene/Cp* group (2.0 Å for N,O compared to 2.4 Å for chlorido). Torsion angles about the imine bond are observed to be 179°, confirming a *trans*-configuration of the imine. Selected bond lengths and angles are given in Table 1 and the crystallographic information is provided in Table 2.

Table 1 Selected bond lengths and angles of complexes **11**–**13**

	Bond distance (Å)/angle (°)		
Entity	**11**	**12**	**13**
M–N	2.088 (2)	2.109 (2)	2.095 (3)
M–Cl	2.4288 (8)	2.4258 (9)	2.4210 (9)
M–O	2.0594 (18)	2.068 (2)	2.084 (2)
N–M–O	88.01 (7)	88.42 (8)	88.02 (10)
N–M–Cl	89.89 (9)	85.18 (7)	85.59 (7)
O–M–Cl	85.38 (6)	88.89 (7)	85.58 (7)
C=N–C–C	179.9 (3)	179.9 (3)	178.7 (3)

In vitro cytotoxicity studies

Complexes synthesised in this study were pre-screened for cytotoxicity in the MCF7 carcinoma breast cancer cell line at an initial dose concentration of 20 µM. This concentration was chosen based on the National Cancer Institute (NCI, USA) criteria which considers compounds with $IC_{50} \leq 20$ µg/mL as having better potential as anticancer drug leads [36]. Cisplatin was used as the positive control in this study. To compare the cytotoxicity at the tested concentration, cell viability was determined using the MTT assay [37, 38].

The anticancer data obtained for complexes **5**–**16** are illustrated in Fig. 3. In general, the ruthenium (**8**, **11** and **14**) and iridium complexes (**10** and **13**) showed greater activity than their rhodium (**9**, **12** and **15**) counterparts. With the exceptions of **8**, **9** and **15**, the complexes were found to

Table 2 Selected crystallographic data and refinement for complexes **11**–**13**

	11	**12**	**13**
Empirical formula	$C_{24}H_{23}ClF_3NORu$	$C_{24}H_{24}ClF_3NORh$	$C_{24}H_{24}ClF_3IrNO$
Formula weight	534.95	537.80	627.11
Temperature (K)	110	173	173
Space group	$P2_1/c$	$P2_1/c$	$P2_1/c$
Unit cell dimensions			
a (Å)	9.6891 (5)	11.8815 (14)	7.7409 (6)
b (Å)	13.8341 (7)	24.057 (3)	22.0339 (15)
c (Å)	16.7075 (7)	7.8436 (10)	12.9297 (9)
α (°)	90	90	90
β (°)	96.279 (1)	103.124 (3)	95.103 (2)
γ (°)	90	90	90
V (Å^3)	2226.04 (19)	2183.4 (5)	2196.6 (3)
Z	4	4	4
Density (calc.) (g cm^{-3})	1.596	1.636	1.896
F(000)	1080	1088	1216
Crystal size (mm)	0.07 × 0.08 × 0.08	0.13 × 0.14 × 0.15	0.09 × 0.13 × 0.16
Theta min–max (°)	1.9, 27.9	1.7, 28.0	1.8, 28.0
Data set	− 12:12; − 18:18; − 21:21	− 15:15; − 31:31; − 10:9	− 10:10; − 29:29; 17:17
Total reflections	43,241	26,557	44,304
Unique reflections	5332	5269	5291
Min. and max. res. dens. (eÅ^{-3})	− 0.52, 0.46	− 0.55, 0.60	− 0.59, 0.96

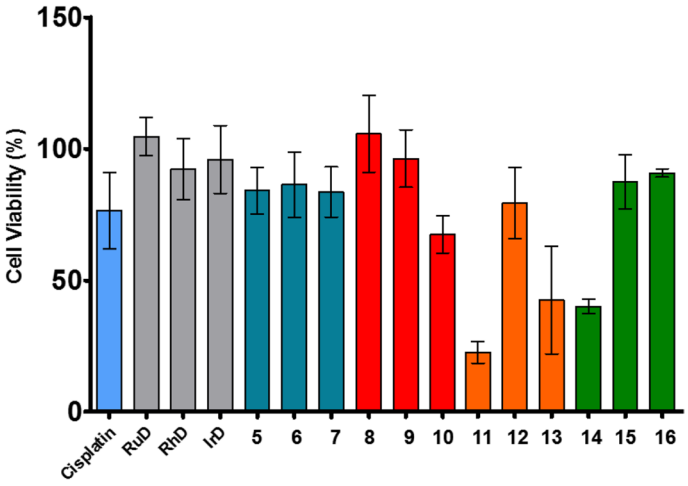

Fig. 3 In vitro activity of complexes **5**–**16** against the MCF7 breast cancer cell line at 20 µM

Table 3 In vitro activity of compounds **11**, **13** and **14** against the MCF7 breast cancer cell line

	IC_{50} (MCF7) (µM)	IC_{50} (CHO) (µM)	SI (IC_{50} (CHO)/IC_{50} (MCF7))
11	17 ± 1.2	6 ± 0.6	0.3
13	21 ± 1.3	96 ± 6.0	4.6
14	19 ± 1.2	84.0 ± 17.7	4.3

be more active than the free metal dimers. This provides evidence that the addition of the salicylaldimine group increases the cytotoxicity of the metals tested. Four complexes (**10**, **11**, **13** and **14**) displayed greater cytotoxicity than cisplatin at 20 µM, against MCF7 cells, with the most active complex being **11**. Complexes bearing the trifluoromethane (**11**–**13**) and trimethylsilane (**14**, **16**) substructure were more active than complexes with the propyl and ferrocenyl (**5**–**10**) salicylaldimine ligand. Ligands **3** and **4** both have higher *C*log*P* values (4.42 and 3.89, respectively) than **1** and **2** (2.50 and 3.33 [39], respectively), suggesting that cytotoxicity is linked to the degree of lipophilicity. Complexes **11**, **13** and **14** showed promise in the pre-screen, and these complexes were taken further to a multi-dose screen to determine their IC_{50} values. The results are shown in Table 3. Complex **11** was found to be the most active, with an IC_{50} value of 16.83 µM. Changing from the ruthenium *p*-cymene (**11**) to the iridium Cp* (**13**) moiety results in an IC_{50} of 20.75 µM. This suggests that the metal fragment plays an important role in the cytotoxicity exhibited in MCF7 cells. In changing the ligand from trifluoromethane (**11**) to trimethylsilane (**14**) in the ruthenium complexes, a slight drop in cytotoxicity was also observed (16.83–19.48 µM, respectively). Compound **11** bears the ligand with the greatest *C*log*P* value (4.42), which could suggest greater accumulation in the cells and therefore greater interaction with intracellular targets. To evaluate their selectivity, the compounds were also tested against non-cancerous Chinese hamster ovarian (CHO) cells. Complexes **13** and **14** showed lower toxicity in the CHO cells than in the MCF7 cell line, with IC_{50} values above 80 µM, which is inactive according to the NCI [36]. Complex **11** was found to be more active in the CHO cells (IC_{50} = 5.67 µM) than in the MCF7 cells (IC_{50} = 16.83 µM). The selectivity index (SI) of these complexes can give insight into which cell line is more sensitive to the complexes. The selectivity index shows that complex **11** has a greater selectivity for non-tumorous cells (SI = 0.34), which suggests that complex **11** may not be a suitable candidate for further testing as a potential anticancer drug. Larger selectivity indices were obtained for complexes **13** and **14** (SI > 4), suggesting that these complexes may be more selective towards cancerous cells and may be potential candidates for further testing.

Stability in DMSO and Interactions with DNA model 5′-GMP

Stability in media is an important feature to identify active species, mechanism of action and potential drug candidates [40]. The stability of complexes **11** and **13** was investigated by ^{1}H NMR spectroscopy in DMSO-d_6 to simulate the chemical environment prior to cell viability studies. The ^{1}H NMR spectrum of **11** shows that after 24 h, a new species had formed (Fig. 4). Signals for the salicylaldimine group were observed to double up, a further evidence that a new species had formed. Splitting of the imine resonance of **11** was observed. No significant change from 24 to 48 h was observed, suggesting that the formation of the new species had reached equilibrium with **11** within 24 h. In contrast to the ruthenium case, the iridium compound **13** showed greater stability in DMSO-d_6 under these conditions. The stacked ^{1}H NMR spectra of **13** in DMSO-d_6 at 24 h intervals are shown in Fig. 4. No additional signals were observed within the 48 h testing period. Integration of the signals after 48 h in DMSO-d_6 for **13** is consistent with the reported

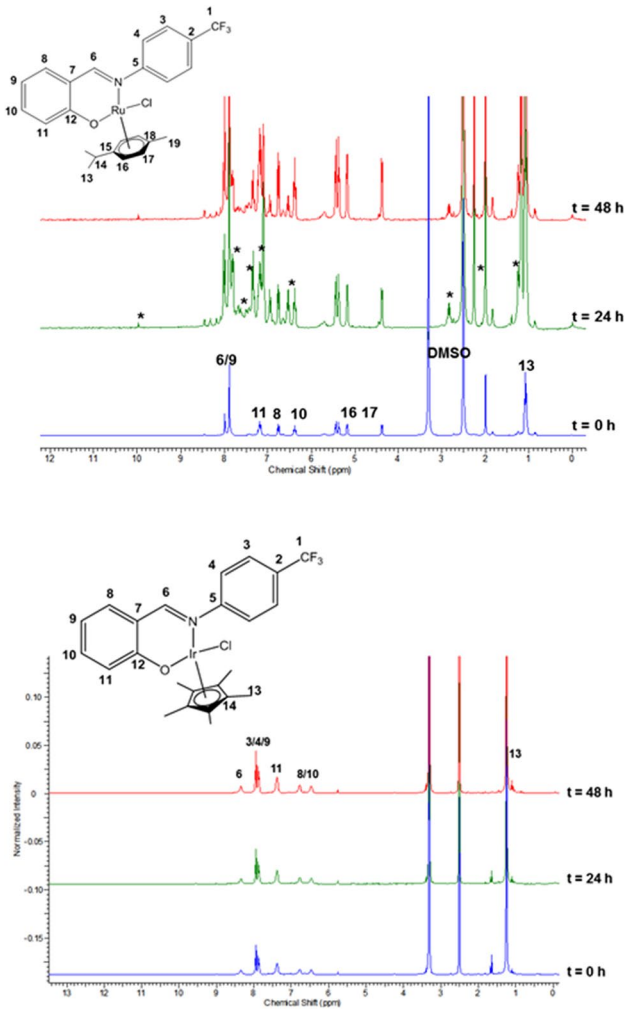

Fig. 4 ^{1}H NMR spectral comparison of **11** (above) and **13** (below) over a 48 h period in DMSO-d_6; sampling taken at 24 h intervals

experimental data. The results obtained in this study suggest that the ruthenium complex (**11**) undergoes solvation and the resulting complex might be responsible for the cytotoxicity observed in the MTT assay. In contrast to this, the iridium complex (**13**) does not undergo solvation, which suggests that this complex is likely to be the active species.

The behaviour of the aforementioned complexes was also studied in partial aqueous solutions to mimic biological conditions. NaCl was used to mimic the salt concentration outside the cells in the body [41]. Complex **11** was analysed for its aqueous stability. A shift in the imine resonance was observed when a high concentration of both H_2O and NaCl is present, suggesting there is a change in the species present in solution. A downfield shift, as well as a change in the splitting pattern of the *p*-cymene proton resonances, is observed which strongly suggests substitution of the labile Cl ligand with DMSO-d_6 or H_2O, as both are coordinating solvents. Since the biological assay medium contains a range of salts and is mainly constituted of H_2O, there is a high likelihood that the active complex is different from the complex that is initially isolated. Complex **13**, though stable in DMSO, was found to form a new species in the different mixtures of DMSO and H_2O. Cleavage of the imine bond was observed when high concentrations of H_2O were present, supported by the appearance of the CHO signal in the ^{1}H NMR spectra. The Cp* signal was observed at 1.25 and 1.18 ppm for the DMSO-d_6:H_2O and 150 mM NaCl(*aq*) samples, respectively, which differs from the DMSO-d_6 sample at 1.23 ppm. Two signals are observed for the Cp* suggesting that the active species may not be the complex isolated initially.

Guanosine 5′-monophosphate disodium (5′-GMP) is a simplistic model used to study possible nucleotide interactions with complexes. Complex **11**, the most active complex, was reacted with 5′-GMP in a DMSO-d_6:H_2O mixture, at 37 °C over 48 h, to understand the interactions with nucleotides. Free GMP was studied under the same conditions and was observed to have no change from the initial ^{1}H NMR spectrum. Ruthenium complexes have been reported to bind to single-stranded DNA via nitrogen donor atoms from guanosine [42–44]. Complex **11** was analysed for its GMP binding affinity using ^{1}H NMR spectroscopy (Fig. 5). A distinctive shift in the proton signals of the arene coordinated to the metal centre indicated a change in the metal centre environment. The aqua product of the complex observed in the aqueous stability study was observed in the **11**–GMP mixture; however, this product is minor. A shift of the proton resonance at 8.0 ppm strongly supports the coordination of the complex at the N7 atom. This result is consistent with the reported shift in the 5′-GMP proton signals for ruthenium–GMP products [42]. This suggests why **11** is very active against both cell lines tested, as this mechanism is not specific to cancerous cells only. The binding of **11** and GMP, and the aqua species formed, suggests that an aqua species is formed before **11** binds to the nucleotide. A similar mechanism is observed for cisplatin [45], which could explain the high levels of toxicity towards healthy cells.

Conclusions

Two new series of trifluoromethane (**11**–**13**) and organosilane (**14**–**16**) complexes bearing Ru(II), Rh(III) or Ir(III) metal centres, derived from two salicylaldimine ligands (**3** and **4**), were synthesised and characterised. Single crystals of **11**–**13** were analysed by X-ray diffraction and further confirmed the molecular structures of the complexes in the solid state. Compounds were characterised using NMR and IR spectroscopies, elemental analysis and EI or ESI mass spectrometry and correlate well with the proposed structures.

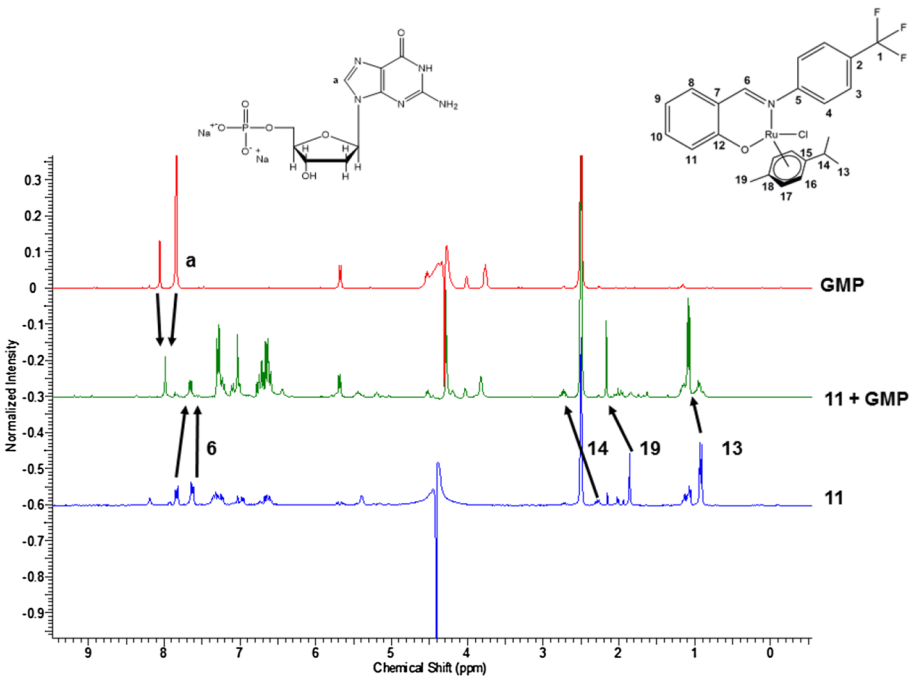

Fig. 5 ^{1}H NMR spectra of **11** and 5′-GMP after 48 h in a DMSO-d_6 and H_2O mixture at 37 °C

The cytotoxicity of compounds **5**–**16**, as well as the dimeric metal precursors, was evaluated against the MCF7 breast carcinoma cell line. Complexes **11**, **13** and **14** exhibited the highest activity in this cell line, with IC_{50} values of 16.83, 20.75 and 19.48 μM observed, respectively. The activity of these complexes can be linked to the lipophilicity of their ligands (the greater the *C*log*P* value of the ligand of the complex, the greater is the cytotoxicity observed). The most active complexes were also evaluated against the Chinese hamster ovarian (CHO) cell line as a representative of normal, healthy cells. Complex **11** was highly active against the CHO cells ($IC_{50} = 5.67$ μM), whilst the other two complexes (**13** and **14**) displayed lower toxicity ($IC_{50} > 80$ μM).

A possible mechanism of action for **11** and **13** was investigated using ^{1}H NMR spectroscopy in DMSO-d_6, DMSO:H_2O and NaCl(*aq*). Doubling of signals in the spectrum of complex **11** suggested low stability in DMSO-d_6; however, complex **13** was found to be inert. Aqua and DMSO species of **11** and **13** were observed after 48 h in DMSO-d_6:H_2O mixtures. Complex **11** showed evidence of binding to 5′-GMP, suggesting a possible mechanism of action similar to cisplatin; however, further studies are needed to verify this.

Acknowledgements Financial support from the University of Cape Town (UCT) and the National Research Foundation (NRF) of South Africa and the Medical Research Council (MRC) of South Africa is gratefully acknowledged. Dr Serah Kimani and Ms Sandra Jordaan are thanked for their contributions.

References

1. Perone M (1884) Ann Chem Pharm 51:1–29
2. Rosenberg B, VanCamp L, Trosko JE, Mansour VH (1969) Nature 222:385–386
3. Bhandari PR (2012) J Adv Pharm Technol Res 3:202–209
4. Hartinger CG, Metzler-Nolte N, Dyson PJ (2012) Organometallics 31:5677–5685
5. Zhang P, Sadler PJ (2017) J Organomet Chem 839:5–14
6. Bergamo A, Masi A, Peacock A, Habtemariam A, Sadler PJ, Sava G (2010) J Inorg Biochem 104:79–86
7. Berndsen RH, Weiss A, Abdul UK, Wong TJ, Meraldi P, Griffioen AW, Dyson PJ, Nowak-Sliwinska P (2017) Sci Rep 7:43005
8. Lucas SJ, Lord RM, Wilson RL, Phillips RM, Sridharan V, McGowan PC (2012) Dalton Trans 41:13800–13802
9. Lucas SJ, Lord RM, Basri AM, Allison SJ, Phillips RM, Blacker AJ, McGowan PC (2016) Dalton Trans 45:6812–6815
10. Yang J, Shi R, Zhou P, Qiu Q, Li H (2016) J Mol Structure 1106:242–258
11. Stringer T, Hendricks DT, Guzgay H, Smith GS (2012) Polyhedron 31:486–493
12. Correia I, Roy S, Matos CP, Borovic S, Butenko N, Cavaco I, Marques F, Lorenzo J, Rodríguez A, Moreno V, Pessoa JC (2015) J Inorg Biochem 147:134–146
13. Govender P, Sudding LC, Clavel CM, Dyson PJ, Therrien B, Smith GS (2013) Dalton Trans 42:1267–1277
14. Rahman FU, Ali A, Khan I, Guo R, Chen L, Wang H, Li ZT, Lin Y, Zhang DW (2015) Polyhedron 100:264–270
15. Rahman FU, Ali A, Guo R, Wang WK, Wang H, Li ZT, Lin Y, Zhang DW (2015) Dalton Trans 44:9872–9880
16. Sharma V, Beatty A, Wey SP, Dahlheimer J, Pica CM, Crankshaw CL, Bass L, Green MA, Welch MJ, Piwnica-Worms D (2000) Chem Biol 7:335–343

17. Stringer T, Taylor D, Guzgay H, Shokar A, Au A, Smith PJ, Hendricks DT, Land KM, Egan TJ, Smith GS (2015) Dalton Trans 44:14906–14917
18. Nkoana W, Nyoni D, Chellan P, Stringer T, Taylor D, Smith PJ, Hutton AT, Smith GS (2014) J Organomet Chem 752:67–75
19. Govender P, Renfrew AK, Clavel CM, Dyson PJ, Therrien B, Smith GS (2011) Dalton Trans 40:1158–1167
20. Rahman FU, Ali A, Guo R, Zhang YC, Wang H, Li ZT, Zhang DW (2015) Dalton Trans 44:2166–2175
21. Isanbor C, O'Hagan D (2006) J Fluor Chem 127:303–319
22. Adams M, Barnard L, de Kock C, Smith PJ, Wiesner L, Chibale K, Smith GS (2016) Dalton Trans 45:5514–5520
23. Adams M, de Kock C, Smith PJ, Land KM, Liu N, Hopper M, Hsiao A, Burgoyne AR, Stringer T, Meyer M, Wiesner L, Chibale K, Smith GS (2015) Dalton Trans 44:2456–2468
24. Kühnert J, Ecorchard P, Lang H (2008) Eur J Inorg Chem 2008:5125–5137
25. Ornelas C (2011) New J Chem 35:1973–1985
26. Kirk KL (2006) J Fluor Chem 127:1013–1029
27. Temmink OH, Emura T, De Bruin M, Fukushima M, Peters GJ (2007) Cancer Sci 98:779–789
28. Bennett MA, Huang TN, Matheson TW, Smith AK, Ittel S, Nickerson W (2007) 16. (η^6-Hexamethylbenzene)ruthenium complexes. In: Inorganic Syntheses, Wiley, Hoboken, pp 74–78
29. White C, Yates A, Maitlis PM, Heinekey DM (2007) (η^5-Pentamethylcyclopentadienyl)rhodium and -iridium compounds. In: Inorganic Syntheses, Wiley, Hoboken, pp 228–234
30. Maqeda L, Makhubela BCE, Smith GS (2015) Polyhedron 91:128–135
31. SAINT Version 7.60a (2006) Bruker AXS Inc., Madison
32. Sheldrick GM (2004) SHELXS-97, SHELXL-2014 and SADABS version 2.05, University of Göttingen, Germany
33. Barbour LJ (2001) J Supramol Chem 1:189–191
34. Atwood JL, Barbour LJ (2003) Cryst Growth Des 3:3
35. Carmichael J, DeGraff WG, Gazdar AF, Minna JD, Mitchell JB (1987) Cancer Res 47:943–946
36. Srisawat T, Chumkaew P, Heed-Chim W, Sukpondma Y, Kanokwiroon K (2013) Trop J Pharm Res 12:71–76
37. Mosmann T (1983) J Immunol Methods 65:55–63
38. Abate G, Aseffa A, Selassie A, Goshu S, Fekade B, WoldeMeskal D, Miörner H (2004) J Clin Microbiol 42:871–873
39. Stringer T, Taylor D, de Kock C, Guzgay H, Au A, An SH, Sanchez B, O'Connor R, Patel N, Land KM, Smith PJ, Hendricks DT, Egan TJ, Smith GS (2013) Eur J Med Chem 69:90–98
40. Shin YG, Bolton JL, van Breemen RB (2002) Comb Chem High Throughput Screen 5:59–64
41. Prough DS, Bidani A (1999) Anesthesiology 90:1247–1249
42. Burgoyne AR, Kaschula CH, Parker MI, Smith GS (2016) Eur J Inorg Chem 2016:1267–1273
43. Scolaro C, Chaplin AB, Hartinger CG, Bergamo A, Cocchietto M, Keppler BK, Sava G, Dyson PJ (2007) Dalton Trans 43:5065–5072
44. Dorcier A, Dyson PJ, Gossens C, Rothlisberger U, Scopelliti R, Tavernelli I (2005) Organometallics 24:2114–2123
45. Reedijk I (2009) Eur J Inorg Chem 2009:1303–1312